Supporting Information

Sun et al. 10.1073/pnas.1101101108

SI Materials and Methods

Bacterial Strains, Plasmids, and Growth. Plasmids were introduced into *Myxococcus xanthus* by electroporation. Mutants and transformants were obtained by homologous recombination. Complementation, expression of the fusion, and mutant proteins were all obtained after ectopic integration of the genes of interest at the Mx8-phage attachment site in appropriate deletion backgrounds (1). Integration at $Mx8_{att}$ has no effect on cell motility (1, 2).

For phenotypic assays, cells (10 μL) at a concentration of 4×10^9 cfu/mL were spotted on charcoal yeast extract (CYE) plates containing an agar concentration of either 0.5% [favoring twitching (S) motility] or 1.5% [supporting both gliding (A) and twitching motility], incubated at 32 °C, and photographed after 48 h with an Olympus SZ61 binocular or a Nikon Eclipse (model TE2000E) microscope.

Preparation of Solubilized AglRQS Complex. A midexponential phase, a culture of wild type or the AglQ-HA–expressing strain grown in 1L CYE medium was harvested, washed, resuspended in 25 mL lysis buffer [50 mM NaCl, 1 mM EDTA, 200 μg/mL lysozyme, 20 mM Tris-HCl (pH 7.5), 500 U Benzonase, and 10 mM PMSF) and lysed using a French pressure cell press. Cell debris was removed by slow-speed centrifugation. Ultracentrifugation (1 h at 10,0000 × *g*) then was used to pellet the cell membrane containing the AglRQS proteins, and the supernatant corresponding to the soluble fraction was discarded. The membrane pellet was resuspended in 2 mL lysis buffer (without lysozyme) and homogenized with a Potter–Elvehjem homogenizer. Membranes then were solubilized gently with 1% dodecyl maltoside (DDM) for 1 h at 4 °C. Solubilized membranes were ultracentrifuged again, and the soluble fraction containing the solubilized protein complex was subjected to the coimmunoprecipitation procedure.

Coimmunoprecipitation of the AglRQS Complex. Solubilized membranes were mixed with 100 μL anti-HA affinity matrix (Roche) and incubated at 4 °C for 1 h. The beads were washed repeatedly in Y-Buffer [50 mM NaCl, 1 mM EDTA, 20 mM Tris-HCl (pH 7.5)] containing decreasing amounts of DDM (1–0.1%). After washing, the beads were resuspended directly in 100 μL of Laemmli buffer and boiled at 100 °C for 10 min. Eluates were analyzed by SDS/PAGE and stained with Sypro-Ruby (Bio-Rad). As a control, protein lysates from the nontransformed *M. xanthus* wild-type strain were prepared following the same procedure (membrane solubilization and coimmunoprecipitation).

Mass Spectrometry and Data Analysis. After SDS-PAGE and staining of protein lysates from the AglQ-HA fusion protein constructs (wild type or D28N mutant) and nontransformed control, lanes were excised and subjected to antigen retrieval by heating, disulfide reduction, and alkylation with iodoacetamide, in-gel trypsin digestion, and peptide elution (3). Peptides were desalted using microscale reversed-phase chromatography and then were subjected to reversed-phase nano-liquid chromatography (LC)-MS and MS/MS performed on a 2D nano-flow capillary HPLCy system (Eksigent) coupled to an LTQ-Orbitrap hybrid mass spectrometer (ThermoFisher Scientific). Sample concentration and desalting were performed online using a trapping column (180 μm × *ca*. 20 mm) packed with 5 μm 100 Å Magic AQ C18 material (Michrom) at a flow rate of 7 μL/min for 2 min. Separation was achieved using an analytical capillary column (100 μm × *ca*. 100 mm) packed with 3 μm 100 Å Magic AQ C18 material (Michrom) terminating in a pulled sprayer tip, under a linear gradient of buffers A [3% acetonitrile (ACN)/0.1% formic acid (FA)] and B [97% ACN/ 0.1% FA] over 70 min at a flow rate of ~0.5 μL/min. Electrospray ionization was carried out at 2.5 kV, with the LTQ heated capillary set to 200 °C. Full-scan mass spectra were acquired in the Orbitrap in the positive-ion mode over the range *m*/*z* 300–2000 at a resolution of 60,000. Mass accuracy after internal calibration typically was within 2–3 ppm. Simultaneously, MS/MS was acquired using the LTQ for the seven most abundant, multiply charged species in the mass spectrum with signal intensities of >1,000 nL. MS/MS collision energies were set at 35%. Dynamic exclusion was set so that MS/MS for each species was acquired a maximum of once over a period of 120 s. All spectra were recorded in profile mode for further processing and analysis. Xcalibur software (ThermoFisher Scientific) was used for MS and MS/MS data analysis. Peptide and protein assignments were conducted using Mascot (Matrix Science) to search against the *M. xanthus* species subset of the Trembl database, using a error window of 8 ppm on the precursor ions and 1.2 Da on the fragment ions. Fixed modifications were set to include carbamidomethylation of cysteine; variable modifications were set to include oxidation of methionine. Scaffold software (Proteome Software) was used to collate and coalesce database search results.

Kymograph Analysis and Bead Tracking. We used custom software written in Matlab to construct the kymograph. The user selected a region of interest (ROI) that included only one cell image. A 2D matrix then was formed from the intensity profiles along the middle line (axial direction) of the cell image from a time-sequence stack. The 2D matrix was displayed as a pseudocolored image to form the kymograph.

For bead tracking, the original image (ROI) was preprocessed to get uniform background. Next, the mean intensity of the image was subtracted from the image. Then, the image was inverted, and the mean intensity of the inverted image was subtracted. The two subtracted images were added together to form the final image. In this way, the contour and contrast of the cell were greatly enhanced. The final image was segmented with a clustering (*k*-means) algorithm by assuming three clusters, which correspond to the bead (brightest cluster), the cell (second-brightest cluster), and the background (darkest cluster). The areas of the bead and cell were used as secondary criteria to eliminate false segments. The centroids of the segmented cell and bead then were calculated. The movement of the bead relative to the cell was recorded to compensate for any drift of the cell relative to the imaging optics.

Measurement of the Membrane Potential, Intracellular ATP Level, and pH. Typically, *M. xanthus* cells were grown in CYE to $OD_{0.5}$, and each drug was added at the appropriate concentration for 15 min at 32 °C. Then 1 mL of each suspension was centrifuged, and the cell pellets were concentrated 50-fold in 100 mM Tris HCl (pH 7.8) and 1 mM EDTA. After 3-min incubation at 32 °C, each suspension was diluted 20-fold in 100 mM NaPi (pH 7.5), 1 mM KCl, and 0.4% glycerol and was equilibrated at 32 °C for 15 min. ^{3}H-TPP$^+$ was added to the suspension at 10 μM (70,000 cpm) and incubated for 1 h at 32 °C. Incorporated radioactivity in 100 μL of the cell suspension was measured directly on filters after three washes in 100 mM NaPi (pH 7.8) with a Beckman Coulter scintillation counter. Under these conditions (pH 7.8), we determined that $\Delta pH = 0$; thus the proton motive force (PMF) equals the membrane potential (PMF = $\Delta\psi$). The membrane

potential then was calculated using the Nernst equation as previously described (4).

To measure changes in intracellular pH, cells were grown to midexponential phase and mixed with BCEF-AM (0.5 mM, Molecular Probes) before they were transferred to a standard TPM-agar pad (pH 6) on a microscope slide. Nigericin, valinomycin, and carbonyl cyanide-m-chlorophenylhydrazone (CCCP) were injected at appropriate concentrations directly on the microscope. All fluorescence images were captured with a 480-nm excitation filter but with two different emission filters (535 and 610 nm) to monitor changes in intracellular pH. Intracellular pH variations were quantified by calculating R = fluorescence λ535 nm/fluorescence λ610 nm. Emission of BCECF (Molecular Probes) at λ535 nm decreases with intracellular pH; thus any drug that collapses the pH gradient is expected to decrease R, because the pH of the surrounding medium is acidic (pH 6) and the initial intracellular pH is 7.8.

Imaging of Cell Gliding. The microscope was equipped with a "Perfect Focus System" (PFS) that automatically maintains focus so that the point of interest within a specimen is in sharp focus at all times, despite any mechanical or thermal perturbations. Images were recorded with a CoolSNAP HQ 2 (Roper Scientific,) and a 40×/0.75 DLL Plan-Apochromat or a 100×/1.4 DLL objective. All fluorescence images were acquired with a minimal exposure time to minimize bleaching and phototoxicity effects. Before any image processing, phase-contrast or fluorescent gray-scale images used for segmentation were equalized to reduce fluctuations in background noise. Cell tracking was performed automatically. When appropriate to correct tracking errors, manual measurements also were performed with tools built into the software. Images were processed under both ImageJ 1.40g (National Institutes of Health) and MetaMorph.

1. Leonardy S, Freymark G, Hebener S, Ellehauge E, Søgaard-Andersen L (2007) Coupling of protein localization and cell movements by a dynamically localized response regulator in *Myxococcus xanthus*. *EMBO J* 26:4433–4444.
2. Mignot T, Shaevitz JW, Hartzell PL, Zusman DR (2007) Evidence that focal adhesion complexes power bacterial gliding motility. *Science* 315:853–856.
3. Shevchenko A, Tomas H, Havlis J, Olsen JV, Mann M (2006) In-gel digestion for mass spectrometric characterization of proteins and proteomes. *Nat Protoc* 1:2856–2860.
4. Cascales E, Christie PJ (2004) Agrobacterium VirB10, an ATP energy sensor required for type IV secretion. *Proc Natl Acad Sci USA* 101:17228–17233.

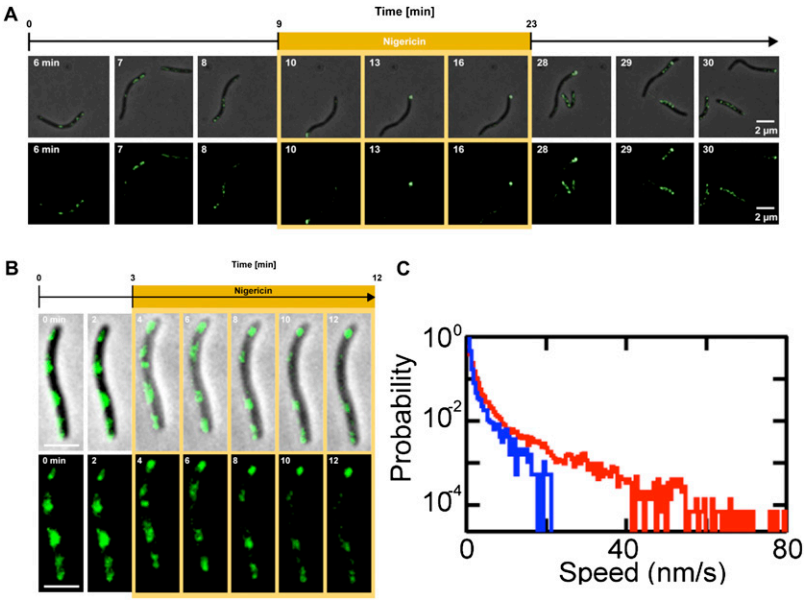

Fig. S1. (*A*) Addition of nigericin (100 μM) rapidly blocks movement and disperses the AglZ-YFP clusters. After washing, movement is resumed coincidently with the reappearance of AglZ-YFP internal clusters. (*B*) Nigericin disperses the AglQ-mCherry clusters. Note the condensation of a polar cluster upon nigericin treatment. (Scale bar, 2 μm.) (*C*) Addition of A22 (50 μg/mL) significantly decreases bead gliding speed (blue) as compared with the speed on nontreated cells (red).

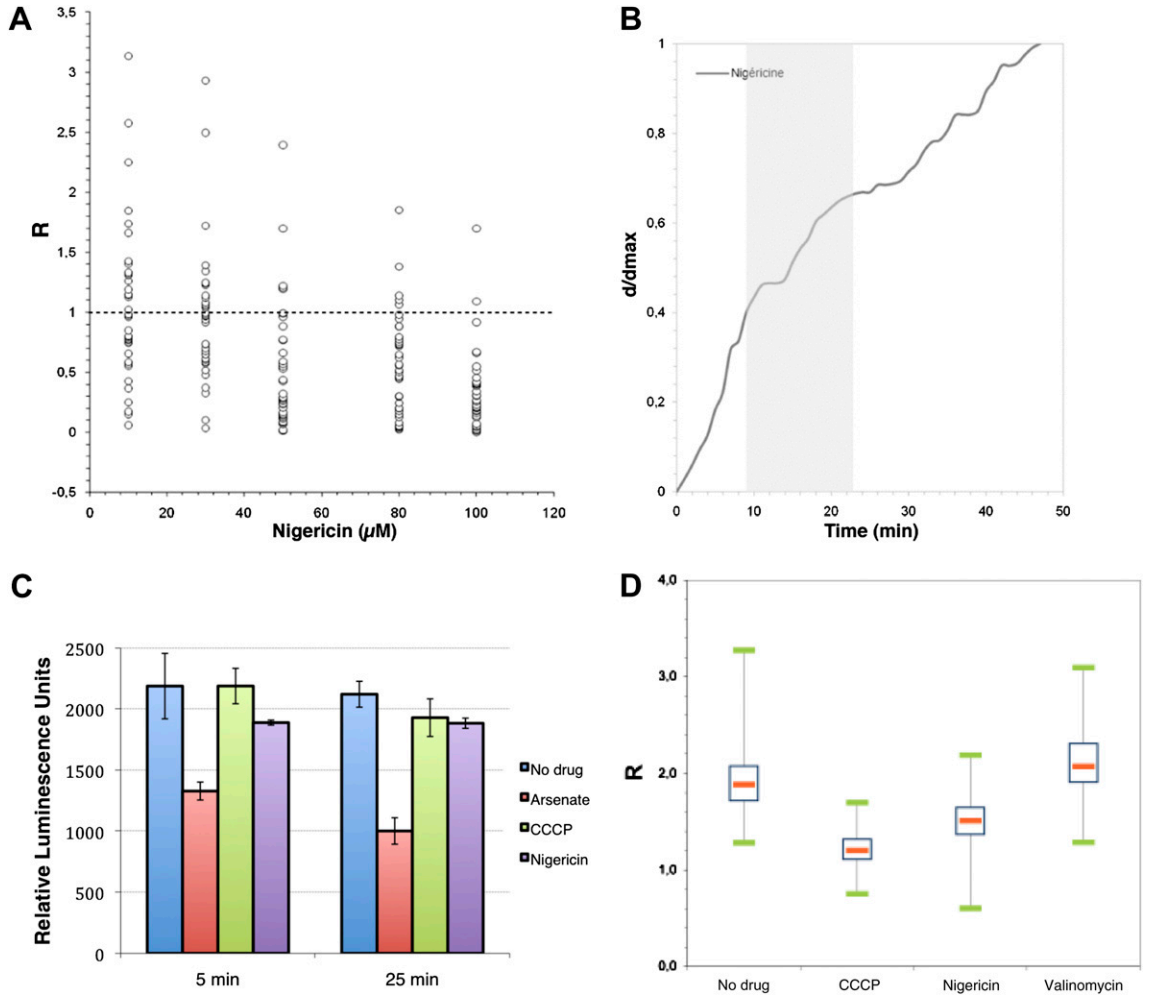

Fig. S2. (*A*) Nigericin affects A motility in a dose-dependent manner. The ratios of the velocity of the cells after treatment with various concentrations of nigericin to the velocity of the cells before treatment (*R*) were calculated (n = 40 cells). (*B*) Nigericin does not affect type IV pilus-dependent S motility. To measure S motility, GFP-labeled cells were mixed at a 1:10 ratio with an A^-S^+ mutant (*aglQ*), and fluorescent cells were tracked within the nonfluorescent population. The d/dmax ratio of a representative cell is shown over time and during nigericin (100 μM) injection. (*C*) Effects of nigericin (100 μM) and CCCP (10 μM) on the intracellular ATP pools. The intracellular ATP levels remain high even after 25 min of nigericin or CCCP treatment. In contrast, arsenate, known to inhibit ATP recycling (1), rapidly affects the ATP intracellular pools. (*D*) After injection of CCCP, nigericin, and valinomycin, changes in intracellular pH were monitored using BCEF. Shown are boxplots of *R* values for calculated for 200 cells in each condition (*Materials and Methods*).

1. Jaffe JD, Miyata M, Berg HC (2004) Energetics of gliding motility in *Mycoplasma mobile*. *J Bacteriol* 186:4254–4261.

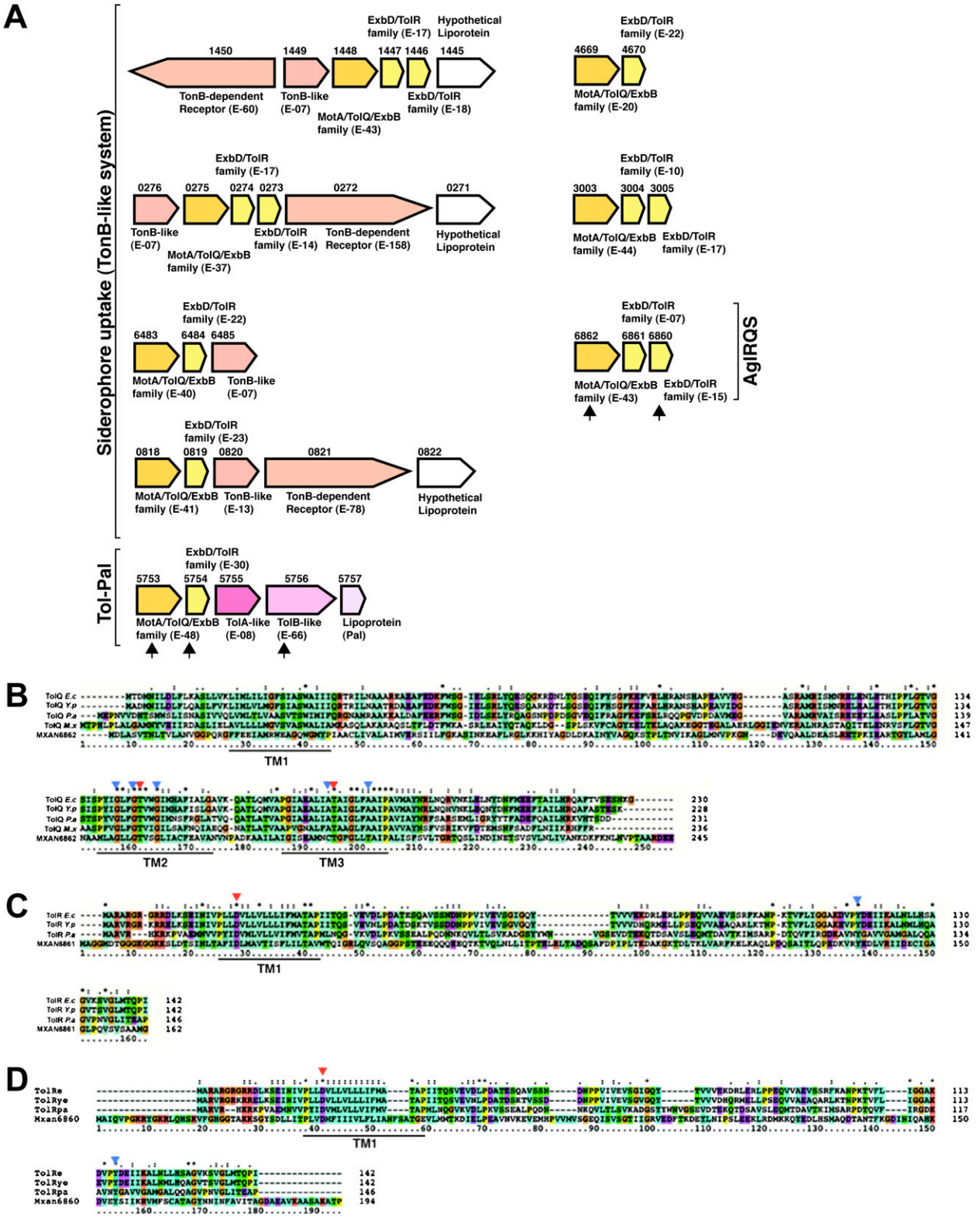

Fig. S3. (*A*) The *Myxococcus* genome contains eight loci carrying genes encoding Tol/Exb/Mot. Four clusters encode TonB-like systems involved in iron siderophore transport (1) and thus were discarded for this analysis. Transposon insertions known to disrupt A motility are shown (black arrows). Three insertions were found in a cluster encoding a complete Tol-Pal system. However, Tol-Pal also is required for S motility (2). In fact, Tol-Pal is involved in membrane integrity, cell division, and protein localization in all systems studied so far (3–5); thus the effects on motility probably are indirect. Blast E values are shown for each predicted gene. (*B–D*) Multiple sequence alignment of AglR, AglQ,. and AglS with TolQ (*B*) and TolR (*C* and *D*) from canonical Tol-Pal systems (Ec: *Escherichia coli*; Yp: *Yersinia pseudotuberculosis*; Ye: *Yersinia enteroccolitica*; Pa: *Pseudomonas aeruginosa*). The critical transmembrane helices are conserved

Legend continued on following page

in all AglRQS proteins. Blue arrows indicate critical residues for channel assembly in *E. coli* TolQ. Note that some of these residues are missing in AglR. Red arrows indicate residues that are essential for proton conductance in *E. coli* TolQR. All these residues are systematically conserved in AglR, -Q, and -S.

1. Postle K, Kadner RJ (2003) Touch and go: tying TonB to transport. *Mol Microbiol* 49:869–882.
2. Youderian P, Burke N, White DJ, Hartzell PL (2003) Identification of genes required for adventurous gliding motility in *Myxococcus xanthus* with the transposable element mariner. *Mol Microbiol* 49:555–570.
3. Lloubès R, et al. (2001) The Tol-Pal proteins of the *Escherichia coli* cell envelope: An energized system required for outer membrane integrity? *Res Microbiol* 152:523–529.
4. Gerding MA, Ogata Y, Pecora ND, Niki H, de Boer PA (2007) The trans-envelope Tol-Pal complex is part of the cell division machinery and required for proper outer-membrane invagination during cell constriction in *E. coli*. *Mol Microbiol* 63:1008–1025.
5. Yeh YC, Comolli LR, Downing KH, Shapiro L, McAdams HH (2010) The caulobacter Tol-Pal complex is essential for outer membrane integrity and the positioning of a polar localization factor. *J Bacteriol* 192:4847–4858.

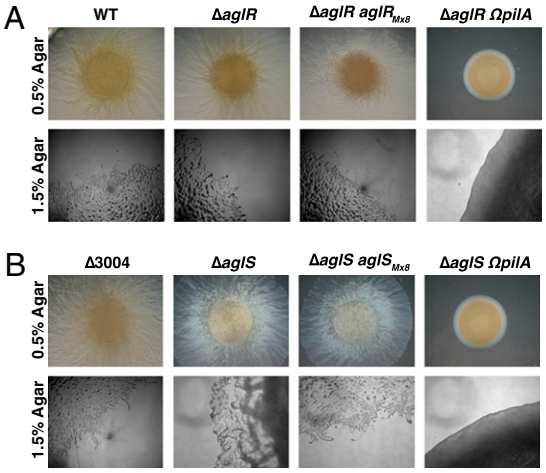

Fig. S4. Both *aglR* and *aglS* are essential for gliding motility. Hard and soft agar motility assays showing motility defects of the *aglR* (*A*) and *aglS* (*B*) deletion mutants. For both mutants, single motile cells are not detected at the colony edges, and combined *pilA* disruption results in complete loss of motility. Both *aglR and aglS* defects are fully complemented when *aglR and aglS* are expressed ectopically from the Mx8 phage attachment site, confirming their respective roles in gliding motility.

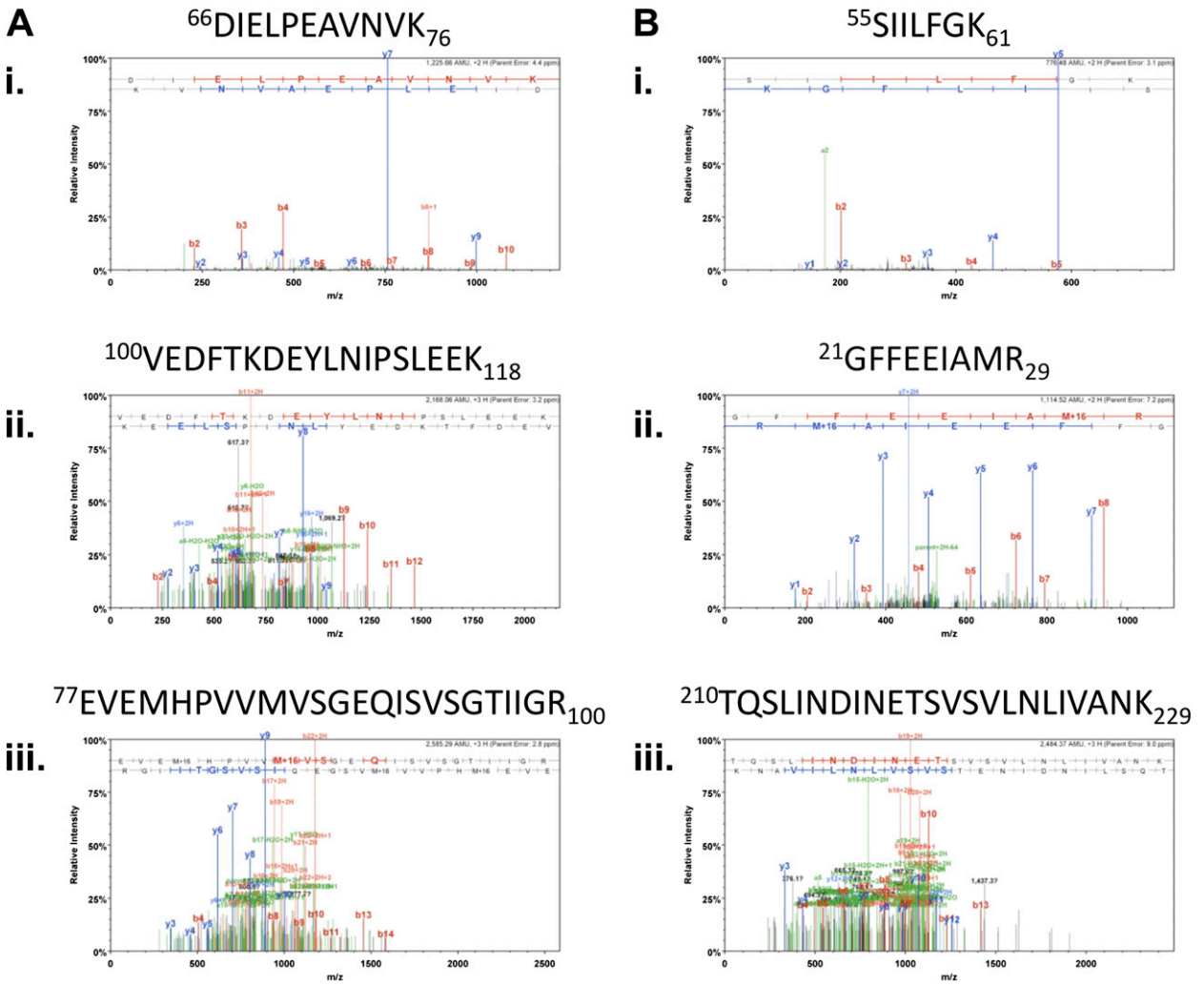

Fig. S5. AglR, -Q, and -S form a complex. Mass spectra from LC-MS of peptides derived from SDS/PAGE analysis of proteins associated with immunoprecipitated AglQ-HA fusion proteins. Prominent detected ions in the spectra are annotated with the theoretical fragment ions of the peptides to which they were assigned by Mascot. Peptide sequences are shown above the spectra. (*A*) Peptides assigned to AglR are (*i*) 66–76, detected as an $[M+2H]^{2+}$ ion at *m/z* 613.8378; (*ii*)100–118, detected as an $[M+^{3}H]^{3+}$ ion at *m/z* 723.6939; and (*iii*) 77–100, detected as an $[M+^{3}H]^{3+}$ ion at *m/z* 862.7707; Mascot scores are 38, 31, and 41, respectively. (*B*) Peptides assigned to AglR are (*i*) 55–61, detected as an $[M+2H]^{2+}$ ion at *m/z* 389.2484; (*ii*) 21–29, detected as an $[M+2H]^{2+}$ ion at *m/z* 558.2672; and (*iii*) 210–229, detected as an $[M+^{3}H]^{3+}$ ion at *m/z* 829.1293; Mascot scores are 19, 53, and 36, respectively. Peptide scores correspond to expectation values <0.05. Consequently, both proteins were assigned a Scaffold confidence score of 100% with no grouping ambiguity.

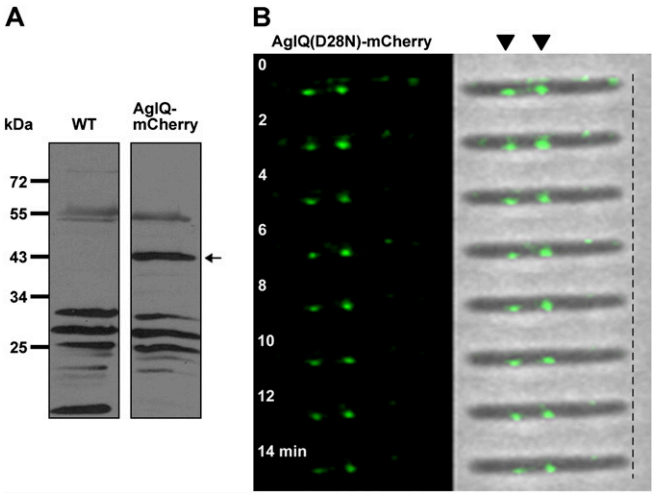

Fig. S6. (*A*) AglQ-mCherry was expressed from its natural promoter at the Mx8 phage attachment site in the AglQ mutant. The chimeric protein promotes motility, albeit at reduced velocities. Western immunoblot using an anti-mCherry antiserum show stable expression of a specific species of expected size. (*B*) AglQ(D28N)-mCherry assembles clusters that are not dynamic.

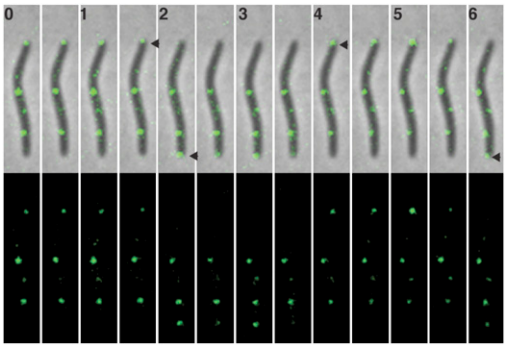

Fig. S7. Localization of AglZ-YFP in an *aglQ* mutant. The AglZ-YFP clusters retain a fixed position at all times, but directional pole-to-pole oscillation still is observed (black arrows). Time is indicated in minutes.

Table S1. Plasmids and strains used in this study

Plasmid or strain	Description	Source
Plasmid		
pBJ114	Used to create deletions, *galK*, KmR	Laboratory collection
pSWU19	KmR used to integrate genes ectopically at mx8att	Laboratory collection
pSWU30	TetR used to integrate genes ectopically at mx8att	Laboratory collection
pBJΔpilA	pBJ114 allowing deletion of *pilA*	Z. Yang
pBJΔaglQ	pBJ114 allowing deletion of *aglQ*	This work
pBJAglZY	pBJ114 with a cassette allowing construction of the *aglZ-YFP* chimeric gene	Laboratory collection
pSWU19aglQHA	pSWU19 allowing expression of *aglQ-HA* from it own promoter at $mx8_{att}$	This work
pSWU19D28NHA	pSWU19 allowing expression of *aglQD28N-HA* from it own promoter at $mx8_{att}$	This work
pSWU19aglQCh	pSWU19 allowing expression of *aglQ-mCherry* from it own promoter at $mx8_{att}$	This work
pSWU30aglQCh	pSWU30 allowing expression of *aglQ-mCherry* from it own promoter at $mx8_{att}$	This work
pSWU19D28NC	pSWU19 allowing expression of $aglQ_{D28N}$-*mCherry* from it own promoter at $mx8_{att}$	This work
pBJΔaglR	pBJ114 allowing deletion of *aglR*	This work
pBJΔaglS	pBJ114 allowing deletion of *aglS*	This work
pSWU30aglR	pSWU30 allowing expression of *aglR* from it own promoter at $mx8_{att}$	This work
pSWU30aglS	pSWU30 allowing expression of *aglS* from it own promoter at $mx8_{att}$	This work
pBJΔ3004	pBJ114 allowing deletion of MXAN3004	This work
Strain	Construction and genotype	
DZ2	Wild type	Laboratory collection
TM9	DZ2 *aglZYFP; aglZ-YFP*	Laboratory collection
TM146	DZ2 Δ*aglQ* (pBJΔaglQ); Δ*aglQ*	This work
TM156	DZ2 *pilA::tet;* Ω*pilA*	This work
TM163	TM146 *aglZYFP* (pBJAglZY); Δ*aglQ aglZ-YFP*	This work
TM251	TM146 *mx8att::aglQHA* (pSWU19aglQHA); Δ*aglQ aglQ-HA*	This work
TM255	TM146 *pilA::tet;* Δ*aglQ* Ω*pilA*	This work
TM295	TM146 *frzE::tn5Ω226;* Δ*aglQ* Ω*frzE*	This work
TM312	TM146 *mx8att::aglQD28NHA* (pSWU19D28NHA); Δ*aglQ aglQD28N-HA*	This work
TM333	TM146 *mx8att::aglQmCherry* (pSWU19aglQCh); Δ*aglQ aglQ-mCherry*	This work
TM348	TM146 *mx8att::aglQmCherry* (pSWU30aglQCh); Δ*aglQ aglQ-mCherry*	This work
TM337	TM255 *mx8att::aglQmCherry* (pSWU19aglQCh); Ω*pilA* Δ*aglQ aglQ-mCherry*	This work
TM340	TM163 *mx8att::aglQmCherry* (pSWU30aglQCh); *aglZYFP* Δ*aglQ aglQ-mCherry*	This work
TM364	TM255 *mx8att::*$aglQ_{D28N}$*mCherry* (pSWU19D28NCh); Δ*aglQ* $aglQ_{D28N}$-*mCherry* Ω*pilA*	This work
TM384	DZ2 Δ*aglR* (pBJΔaglR); Δ*aglR*	This work
TM449	TM384 Δ*pilA* (pBJΔpilA); Δ*aglR* Δ*pilA*	This work
TM452	DZ2 Δ*aglS* (pBJΔaglS); Δ*aglS*	This work
TM450	TM384 *mx8att::aglR* (pSWU30aglR); Δ*aglR aglR*	This work
TM455	TM452 *mx8att::aglS* (pSWU30aglS); Δ*aglS aglS*	This work
TM454	TM452 *pilA::tet;* Δ*aglS* Ω*pilA*	This work
TM363	DZ2 ΔMXAN3004 (pBJΔ3004); ΔMXAN3004	This work

Table S2. Primers

Name	Sequences of primers (5′–3′)
Δ6861–1	AAAGAATTCAATTCCTGTGAGATTTCAGCACTTAAC
Δ6861–2	AAAGGATCCGGCGTTCTTCTCCTTCGGC
Δ6861–3	AAAGGATCCCCGCCCAAGGAGCTCACG
Δ6861–4	TTTAAGCTTCCGCCAGCTTCGTGCC
AglR-3	CGGGATCCGAAGTCCTTCGGGAACCCG
AglR-7	CCCAAGCTTTTAAGCGTAGTCTGGGACGTCGTATGGGTAGCCCATCGCCGCGGACA
AglR-5	GATGAATGCCGTGAGGTTGATGG
AglR-9	CTCACGGCATTCATCAACCTGATGGCGGTGACCATCAG
6861-mCherry-1	GCCCATCGCCGCGGACAC
6861-mCherry-2	GTCCGCGGCGATGGGCGTGAGCAAGGGCGAGGAG
6861-mCherry-3	CCCAAGCTTTTACTTGTACAGCTCGTCCATG
D6862-5	GGAATTCAATCAGCTCCGCCAGGGAC
D6862-6	CGGGATCCCGAGTGTTGCCTCCACAG
D6862-7	CGGGATCCGAAGTCCTTCGGGAACCC
D6862-8	CCCAAGCTTGAGCTTCTCCTCCAGCGACG
D6860-5	GGAATTCAGACGCCGAAGATCGAGGC
D6860-6	CGGGATCCGACGTGTCGTGAGCTCCTTG
D6860-7	CGGGATCCCTTCCAGGTGATTGGGCCTTG
D6860-8	CCCAAGCTTATGAAGGGCTCGCGCTCC
D3004-1	CCGAATTCGCGAAATCACCGAGCAGC
D3004-2	CCGGGAGTAGTGGAACGCC
D3004-3	TTCCACTACTCCCGGACCCTGGGAGCCATCTGAG
D3004-4	CCAAGCTTGATCCTCAGCGCCAACGAG
CgmoA-1	CGGGATCCGAATCCGGCCTTAACACGCG
CgmoA-2	CCCAAGCTTGGCGTTCTTCTCCTTCGGC
CgmoC-1	GAGCTCCTTGGGCGGCGAGTGTTGCCTCCACAGGC
CgmoC-2	CCGCCCAAGGAGCTCAC
CgmoC-3	CCCAAGCTTTCCATCGAGGTCGAAGATG

Table S3. Plasmid construction schemes

Plasmid	Construction scheme*
pBJΔaglQ	Primer pairs Δ6861–1/Δ6861–2 and Δ6861–3/Δ6861–4 were used to amplify a 1-kb fragment upstream and downstream of the *aglQ* ORF. First the upstream fragment was cloned at the EcoRI and BamHI sites of pBJ114. Then the downstream fragment was ligated at the BamHI and HindIII sites of the pBJ114-upstream fragment.
pSWU19aglQHA	A fragment encompassing *aglQ* and the *aglQ* promoter region was amplified from the DZ2 chromosome with primers AglR-3/AglR-7 and cloned at the BamHI and *Hin*dIIII sites of pSWU19.
pSWU19D28NHA	A *aglQ(D28N)HA* allele was generated by splicing by overlapping extension (SOE) PCR fusing a fragment amplified from primers AglR-3/AglR-5 to a fragment amplified from AglR-9/AglR-7 using the DZ2 chromosome as a template. The resulting fragment then was ligated to the BamHI and *Hind*IIII sites of pSWU19.
pSWU19aglQCh	Primers AglR-3/6861-mCherry-1 were used to amplify a *aglQ* fragment and its promoter region from the DZ2 chromosome. Primers 6861-mCherry-2/6861-mCherry-3 were used to amplify the *mcherry* fragment from a plasmid containing the *mcherry* gene. Both fragments were fused by SOE-PCR and cloned at the BamHI and HindIII sites of pSWU19.
pSWU30aglQCh	Primers AglR-3/6861-mCherry-1 were used to amplify the *aglQ* fragment and its promoter from the DZ2 chromosome. Primers 6861-mCherry-2/6861-mCherry-3 were used to amplify the fragment *mcherry* from a plasmid containing the *mcherry* gene. Both fragments were fused by SOE-PCR and cloned at the BamHI and *Hind*III sites of pSWU30.
pSWU19D28NC	A *aglQ-D28N-mCherry* allele was generated by SOE PCR fusing a fragment amplified from primers AglR-3/AglR-5 to a fragment amplified from AglR-9/6861-mCherry-1 using the DZ2 chromosome as a template. The resulting fragment then was fused to a third fragment amplified from primers 6861-mCherry-2/6861-mCherry-3 using a plasmid containing the *mcherry* gene as a template. The resulting fragment then was ligated to the BamHI and *Hin*dIIII sites of pSWU19.
pBJΔaglR	Primer pairs D6862-5/D6862-6 and D6862-7/D6862-8 were used to amplify a 1-kb fragment upstream and downstream from the *aglR* ORF. First the upstream fragment was cloned at the EcoRI and BamHI sites of pBJ114. Then the downstream fragment was ligated at the BamHI and HindIII sites of the pBJ114-upstream fragment.
pBJΔaglS	Primer pairs D6860-5/D6860-6 and D6860-7/D6860-8 were used to amplify a 1-kb fragment upstream and downstream from the *aglS* ORF. First the upstream fragment was cloned at the EcoRI and BamHI sites of pBJ114. Then the downstream fragment was ligated at the BamHI and HindIII sites of the pBJ114-upstream fragment
pSWU30aglR	A fragment encompassing *aglR* and the *aglR* promoter region was amplified from the DZ2 chromosome with primers CgmoA-1/CgmoA-2 and cloned at the BamHI and HindIII sites of pSWU30.
pSWU30aglS	Primers CgmoA-1/CgmoC-1 were used to amplify the promoter of *aglS* from the DZ2 chromosome. Primers CgmoC-2/CgmoC-3 were used to amplify *aglS* from the DZ2 chromosome. Both fragments were fused by SOE-PCR and cloned at the BamHI and EcoRI sites of pSWU30.
pBJΔ3004A	Primer pairs D3004-1/D3004-2 and D3004-3/D3004-4 were used to amplify a 1-kb fragment upstream and downstream from the MXAN_3004 ORF. Both fragments were fused by SOE-PCR and cloned at the EcoRI sites and HindIII sites of pBJ114.

*All plasmid inserts were sequenced to ensure the absence of PCR-introduced mutations.

Table S4. Effects of CCCP, valinomycin, and nigericin on the membrane potential

Drug treatment	Effect on membrane potential Δψ (mV)
No treatment	154
CCCP (10 μM)	0
Valinomycin (40 μM)	0
Nigericin (100 μM)	158

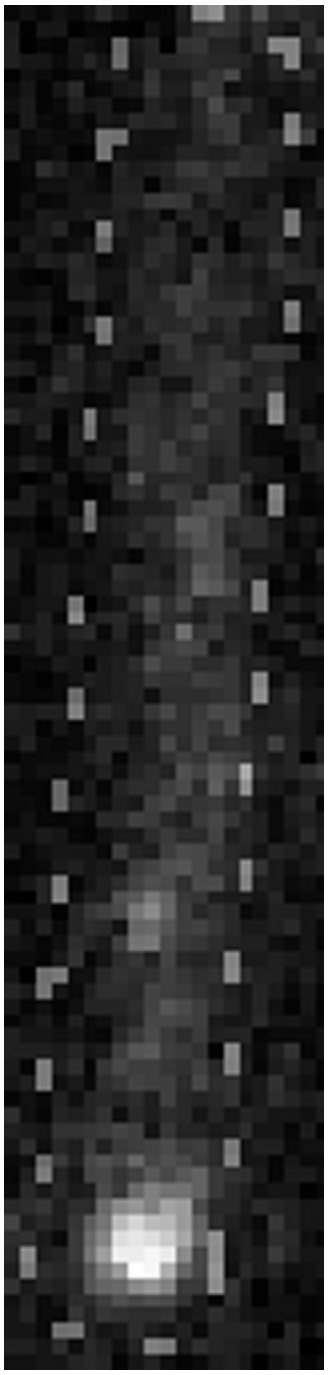

Movie S1. Intracellular transport of AglZ-YFP clusters. Most AglZ-YFP clusters move from the cell head, defined as the brightest pole, toward the back. Some clusters move opposite this direction, and the cell can support both directions of motion at the same time.

Movie S1

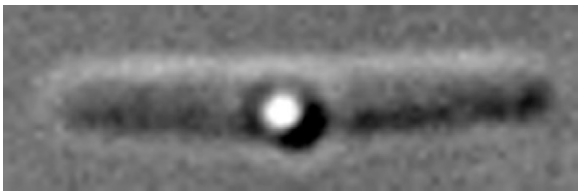

Movie S2. A bead moves along the side of an immobilized cell. Long, unidirectional runs are interrupted by periods of motionless pausing.

Movie S2